IOP Publishing

Photo Acoustic and Optical Coherence Tomography Imaging, Volume 1

Diabetic retinopathy

Ayman El-Baz and Jasjit S Suri

Chapter 1

Computerized tool for the automatic segmentation of DRT edemas using OCT scans

Joaquim de Moura, Plácido L Vidal, Jorge Novo and Marcos Ortega

Diabetic macular edema (DME) is a complication of diabetes mellitus that results from the formation of intraretinal leakage in the macular region. This relevant eye disorder is recognised as a leading cause of visual loss among the industrialized world, as reported in the statistics of the World Health Organization guidelines. This chapter presents a software tool for the automated segmentation of diffuse retinal thickening regions from optical coherence tomography (OCT) images. For this purpose, two retinal regions were defined and extracted: the inner retina and the outer retina. Then, a learning process was used to analyze a comprehensive and heterogeneous subset of relevant patterns in the OCT scans. Finally, two complementary post-processing stages were applied to improve the obtained performance and the overall efficiency of the presented tool. The presented tool achieved satisfactory performance, achieving a Jaccard of 0.6625 and a Dice of 0.7899, which demonstrates the suitability of the adopted solution.

1.1 Introduction

Image processing, analysis and computer vision represent very interesting, interdisciplinary and dynamic scientific fields of computer science [1]. In particular, these relevant areas provide different computational tools that are commonly employed in many technological domains to solve different real-world problems [2]. In this context, after an explosion of interest during the 1980s and 1990s, the last three decades have been characterised by the maturity of these areas and a notable growth in different active applications from different domains of knowledge, such as industry [3], medicine [4], finance [5], engineering [6], agriculture [7] and education [8], among others [9, 10]. Therefore, as a result of this considerable technological advance, we can observe a significant increase in emerging computational solutions that include hardware,

doi:10.1088/978-0-7503-2052-8ch1

software, services and many automatic technologies that have the main objective of improving and facilitating the daily work of specialists and professionals [11, 12].

In particular, in the field of medicine, clinical experts often use different computer-aided diagnosis (CAD) systems for automatic or semi-automatic processing, analysis and recognition of medical images of different types, such as conventional x-ray [13, 14], magnetic resonance [15], computerised tomography [16] or ultrasound scans [17], among others. Therefore, the use of CAD solutions has grown in importance in recent years, facilitating the work of clinicians in diagnostic procedures, avoiding tedious and time-consuming manual procedures.

Specifically in the field of ophthalmology, CAD tools spread rapidly over the years, progressively being integrated into the clinical workflow to assist the clinical specialists in diagnostic, prognostic and therapeutic tasks in daily practice. In this context, these computational tools use the clinical information obtained through different imaging modalities, such as classical retinography [18], fluorescein angiography [19], optical coherence tomography (OCT) [20–22] and optical coherence tomography angiography (OCTA) [23], among others.

OCT is a non-invasive imaging examination widely used in ophthalmology for retinal imaging as well as for morphological analysis of different healthy or pathological structures [24, 25]. This well-established imaging technique uses low-coherence (high-bandwidth) interferometric technology to provide, in real-time, a set of two-dimensional scans of the histological structures of the main ocular tissues via sequential gathering of longitudinal and lateral reflections. In figure 1.1, we can see a representative illustration of a spectral domain OCT system.

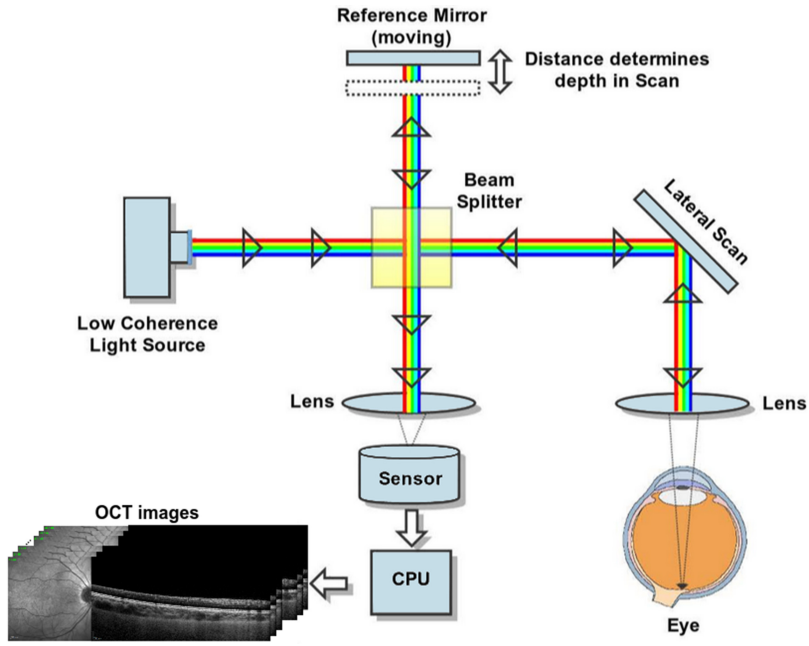

Figure 1.1. Representative illustration of a spectral domain OCT system.

The OCT scans allow a direct high-resolution visualization of the morphology and architecture of the retina and their corresponding histopathological properties. Consequently, these images provide a valuable resource for the detection, diagnosis, and treatments of several eye disorders [26, 27] such as, for example, glaucoma, central serous chorioretinopathy, pigment epithelium detachment, age-related macular degeneration, epiretinal membrane or diabetic macular edema (DME).

With regards to DME, this serious ocular disease is considered a worldwide health concern, in accordance with the World Health Organisation (WHO) guideline statistics [28]. In particular, DME is one of the most important consequences associated with diabetes mellitus, being considered a major cause of vision loss and affects mainly the developed countries. Specifically, figure 1.2 illustrates 6 OCT images showing the presence and absence of DME disease.

Using the OCT imaging as a reference, Otani *et al* [29] proposed a categorisation of DME disease according to three classes: diffuse retinal thickening (DRT), serous retinal detachment (SRD) and cystoid macular edema (CME). To do so, the authors analysed several imaging characteristics of the OCT scans. Subsequently, Panozzo *et al* [30] expanded the existing clinical categorisation by defining new characteristics that can be seen on OCT images and that better characterise this relevant eye disorder. To do this, the authors included information on the volume, diffusion, morphology and presence of the epiretinal membrane. Figure 1.3 illustrates an OCT scan with the three clinical categories of DME analysed.

Regarding the DRT, this type of DME is typically defined by a sponge appearance as a consequence of fluid leakage with restricted reflectivity in the retinal tissues. In addition, since this type of DME usually appears before the SRD and CME regions, it is frequently considered by the clinical experts as a valuable

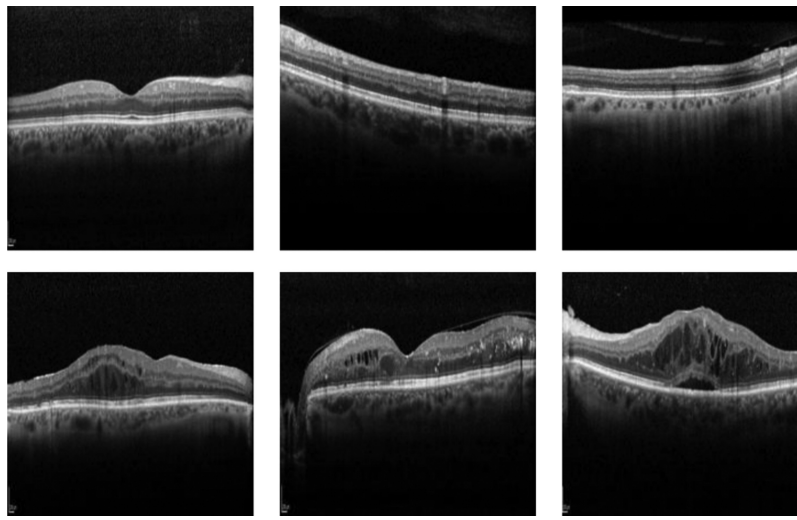

Figure 1.2. Examples of OCT scans. First row, OCT scans of patients without DME disease. Second row, OCT scans of patients with DME disease.

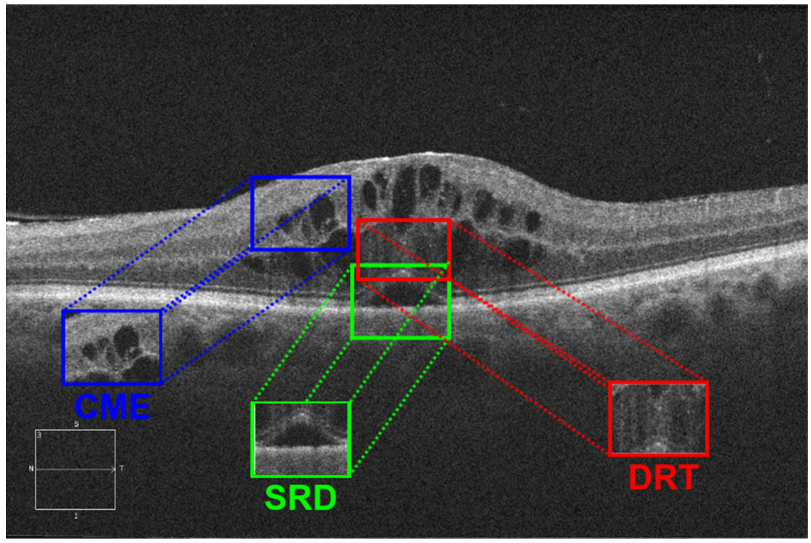

Figure 1.3. OCT image showing the presence of all classes of DME: DRT, CME and SRD.

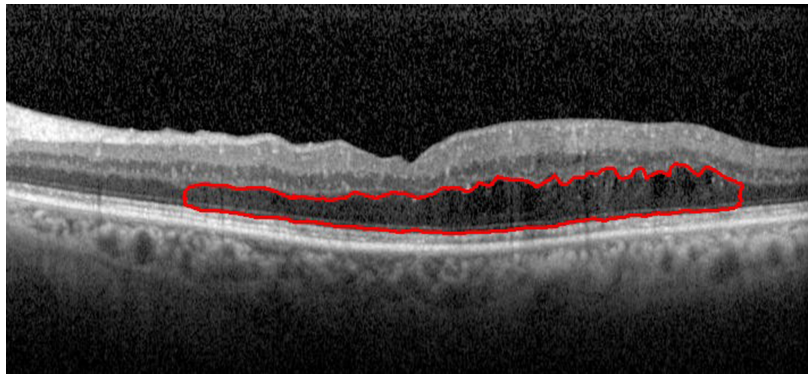

Figure 1.4. OCT scan with the manual delineation of the pathological DRT region.

marker for the diagnosis of this relevant eye disorder [31]. In figure 1.4, we can see an OCT scan with the manual delineation of the pathological DRT region.

Some proposals using OCT scans for the identification, segmentation or characterisation of intraretinal fluid regions associated with DME disorder have been published in recent years. As reference, Gopinath *et al* [32] proposed a strategy for the segmentation of macular edemas in OCT scans. To achieve this, the authors use a convolutional architecture to train a mapping function that captures the output of multiple motions to generate a probability map of the locations of pathological fluids in a given OCT scan. Following a similar strategy, Schlegl *et al* [33] proposed an automatic tool for the quantification of fluid regions in OCT scans by means of different machine learning models. In the work of de Moura *et al* [34], the authors proposed a comprehensive analysis of representative descriptors for the intraretinal

fluid characterization in OCT images. In another proposal [35], the authors presented a novel paradigm to identify fluid accumulations in the retina using intuitive heat maps. Roy *et al* [36] presented a CNN architecture for the segmentation of pathological fluid regions in OCT scans. Samagaio *et al* [37] proposed a novel approach to classify the presence of macular edemas using OCT scans. In another proposal [38], the authors presented an automatic system for the segmentation and characterization of the DME regions in OCT scans. In the work of de Moura *et al* [39], the authors proposed a deep features analysis in a transfer learning-based process for DME screening using OCT scans. Similarly, Chan *et al* [40] proposed a framework based on a transfer learning approach for DME recognition on OCT scans. As we can see from the existing studies, the proposed systems only aimed at identifying areas of intraretinal fluid and, therefore, did not address the identification or segmentation of DRT regions. In this sense, at present, only the works [41, 42] addressed the precise segmentation of DRT regions by OCT scans.

In this chapter, we describe a fully automatic system that identifies and segments DRT edemas from OCT images, following the reference clinical classification in the field of ophthalmology. Firstly, two regions of the retina were automatically delineated: one corresponding to the ILM/OPL region (inner retina) and other to the OPL/RPE region (outer retina). Then, a learning strategy was adopted, analyzing a set of samples of a specific size to extract different feature descriptors. And finally, a post-processing step was applied to improve the overall performance of the presented system.

The chapter is structured as follows: Section 1.2 contains a detailed explanation of the methodology presented. Section 1.3 presents and discusses the obtained results with a brief explanation on their significance. Finally, section 1.4 includes a series of final notes drawn for this research and a commentary on future lines of work.

1.2 Computational identification and segmentation of DRT edemas

The presented pipeline, illustrated in figure 1.5, consists of three main stages: a first stage, in which the main layers of the retina are segmented and two retinal regions are delimited: inner retina and outer retina; a second stage, a set of features within the outer retina is extracted and a machine learning strategy is adapted for the DRT segmentation; a third step, in which a post-processing stage was applied to refine the DRT segmented regions. Each of these stages will be discussed below.

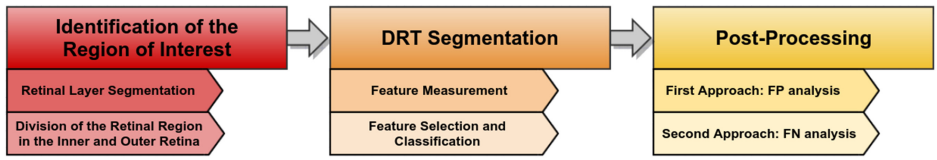

Figure 1.5. Main stages of the automatic segmentation of DRT regions.

1.2.1 Identification of the region of interest

The different types of pathological fluid accumulations are normally found in typical relative positions within the layers of the retina. Specifically, DRT edemas usually occur in the OPL/RPE region. In this way, two regions of the retina were identified, facilitating the subsequent segmentation of this relevant DME type. The following subsections describe this entire process in more detail.

1.2.1.1 Retinal layer segmentation

Regarding the automatic segmentation of the main retinal layers, we followed the previous study of González-López *et al* [43]. In particular, we segment four retinal layers: the inner limiting membrane (ILM), the inner/outer segments (ISOS), the outer plexiform layer (OPL) and the retinal pigment epithelium (RPE). For this purpose, firstly, we used a denoising algorithm based on the Butterworth Fourier filter to mitigate the speckle noise [44], preserving the information contained in the OCT scans. Next, an active contour-based strategy was used to delineate the retinal boundaries. As said, these retinal regions correspond to the region of the retina where the DRT edema usually appears (figure 1.6).

1.2.1.2 Segmentation of the inner/outer retinal regions

Using the segmented retinal layers as reference, two regions are segmented: the ILM/OPL region (inner retina) and the OPL/RPE region (outer retina), as represented in figure 1.7. Based on clinical knowledge, these retinal regions were identified in order to simplify the subsequent DRT segmentation stage.

1.2.2 DRT segmentation

In order to accurately segment the DRT regions, a machine learning algorithm was employed to characterize the pathological regions only in the restricted search space (outer retina). To achieve this, a set of windows of a given size was analyzed, thereby extracting a comprehensive subset of features. Finally, a post-processing step was carried out to improve the results obtained in the segmentation stage. The following subsections describe this entire process in more detail.

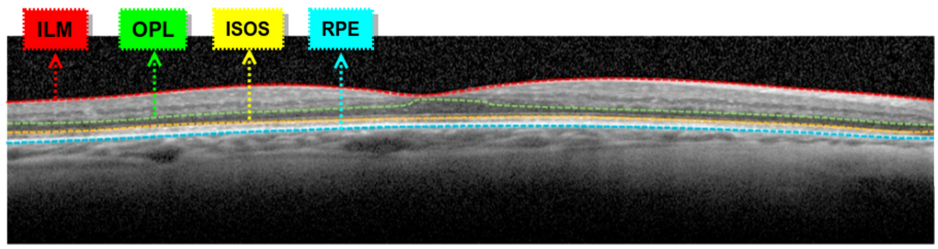

Figure 1.6. Representative example of the retinal layer segmentation stage.

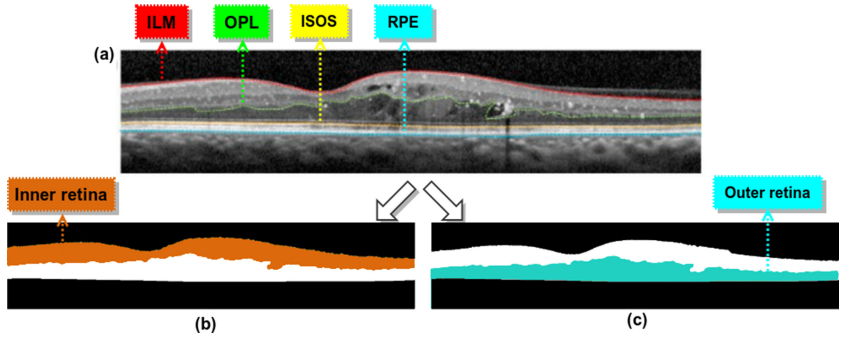

Figure 1.7. Representative example of the segmentation of the inner/outer retinal regions. (a) OCT scan with the main retinal layers segmented. (b) The inner retinal region. (c) The outer retinal region.

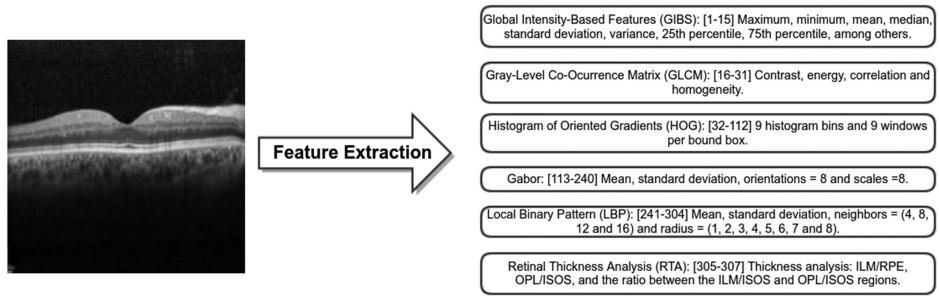

Figure 1.8. Schematic representation of the feature extraction.

1.2.2.1 Feature extraction

To characterize the pathologic patterns of DRT-type edema, a comprehensive set of 307 features was extracted from the outer retinal region, as represented in figure 1.8. In particular, this set of features includes characteristics of intensity, texture and knowledge of the domain.

1.2.2.2 Feature selection and classification

The 307 extracted features were posteriorly analyzed to obtain the subset that maximizes the separability between the DRT and non-DRT regions and, therefore, facilitating the classification process. To do this, we use the well-known Sequence Forward Selection (SFS) [45] algorithm. In particular, this feature selector employs a strategy in which features are sequentially added to a subset of empty candidates until the addition of more features does not decrease the given selection criteria. A machine learning technique is then used to evaluate different prediction models using the previously chosen subset of features. To this end, four classifiers were used to measure the performance of the presented methodology: the Naive Bayes, the Parzen, the Quadratic Bayes Normal Classifier (QDC) and the k-Nearest Neighbors (kNN) for three different k values (k = 3, 5 and 7).

As training details, the initial image dataset was partitioned into two smaller datasets with 50% for training and 50% for testing. In addition, a 10-fold

cross-validation with 50 repetitions was performed. As a final result of this classification stage, all columns in the outer retinal region were categorized into DRT or non-DRT categories.

1.2.3 Post-processing

In this stage, two independent post-processing approaches were designed to improve the results obtained by the presented system. In the following subsections, this whole process is described in more detail.

1.2.3.1 First approach: FP analysis

The first post-processing approach focuses on the analysis and subsequent reduction of the false positive rates. In this sense, these false detections of DRT columns usually occur due to the presence of other pathological structures of similar appearance that can be observed in the outer retinal region. To do this, we implemented a strategy that calculated the minimum width of each segmented region with respect to the nearest corresponding region, thus eliminating small isolated regions, as represented in figure 1.9.

1.2.3.2 Second approach: FN analysis

The second post-processing approach focuses on the analysis and subsequent mitigation of the false negative rates. In particular, these misclassified regions are mainly derived from the presence of speckle noise and/or vascular shadows in the outer region of the retina. To achieve this, we implemented a strategy based on an aggregation factor (d). Specifically, this strategy joins two contiguous regions if the distance between them is less than a predefined aggregation factor, as represented in figure 1.10.

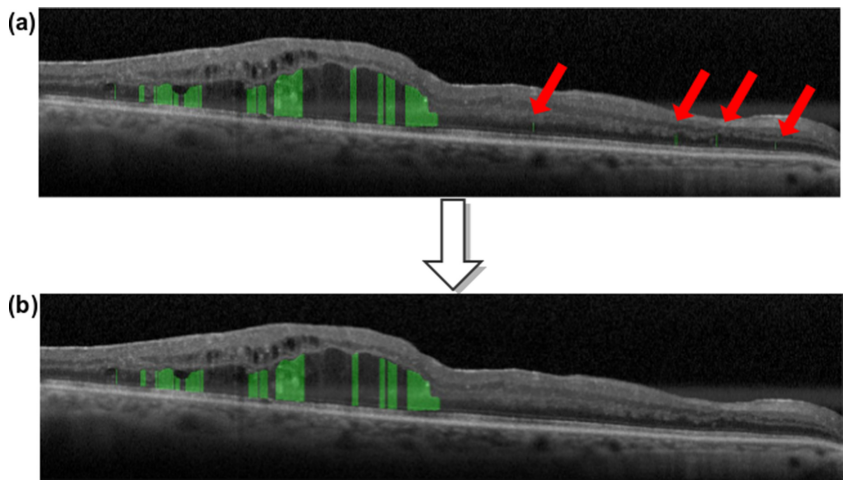

Figure 1.9. Representative example of the first post-processing step. (a) DRT regions without the post-processing step. (b) DRT regions with the post-processing step.

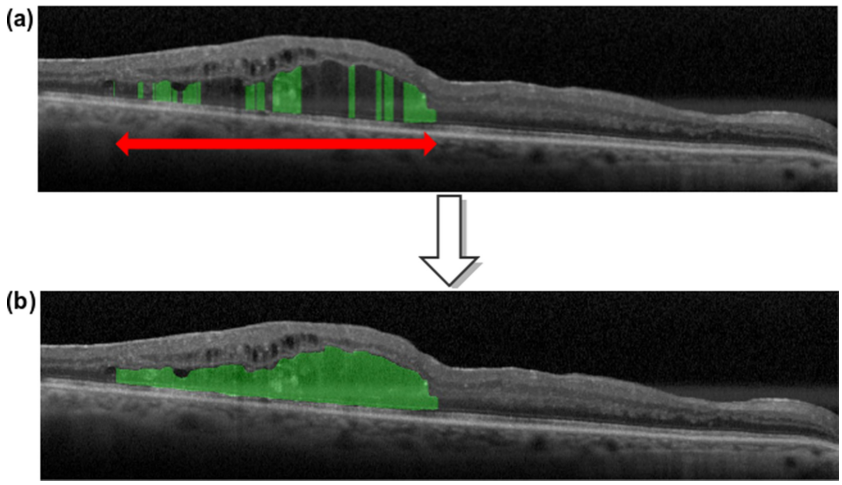

Figure 1.10. Representative example of the second post-processing step. (a) DRT regions without the post-processing step. (b) DRT regions with the post-processing step.

1.3 Results and discussion

The presented method was validated using an image dataset consisting of 70 scans. These scans were obtained using an OCT confocal scanning laser ophthalmoscope (cSLO) imaging device from Heidelberg Spectralis. All the OCT scans were obtained focusing on the macular region of patients diagnosed with DME. In addition, this dataset has a variable resolution that ranges from 401 × 1015 to 481 × 1521 pixels. To ensure the complete anonymity and confidentiality of participants in this study, we used anonymised data images available for research purposes.

To validate the presented methodology, an expert clinician labeled 560 samples to represent the presence of DRT edemas, including 280 for each category, DRT and non-DTR columns. As said, the used dataset was partitioned into 2 subsets, 50% for training and 50% for testing. In addition, we performed a 10-fold cross-validation with 50 repetitions without any pre-processing stage on the input OCT images. In particular, the presented system was evaluated by means of the Accuracy, Jaccard and Dice coefficients, described in equations (1.1), (1.2) and (1.3), respectively.

$$\text{Accuracy} = \frac{\text{TP} + \text{TN}}{\text{TP} + \text{TN} + \text{FP} + \text{FN}} \tag{1.1}$$

$$\text{Jaccard} = \frac{\text{TP}}{\text{TP} + \text{FP} + \text{FN}} \tag{1.2}$$

$$\text{Dice} = \frac{2 \times \text{TP}}{2 \times \text{TP} + \text{FP} + \text{FN}} \tag{1.3}$$

Firstly, we analyze the subset of features that maximizes the separability between the DRT and non-DRT regions. To do this, we use an SFS algorithm to analyze the

initial set of 307 features. As a result of this feature analysis, we can conclude that most of the features were selected from the HOG, Gabor and LBP. Figure 1.11 shows the results obtained with different classifier configurations using a subset of features that was obtained by the SFS algorithm.

Once the best subset of features has been determined, we analyze the different classifiers considered in this work to determine which best discriminates between DRT and non-DRT regions. Figure 1.12 presents the results obtained by each classifier using the most relevant subset of features. As we can see, the best results

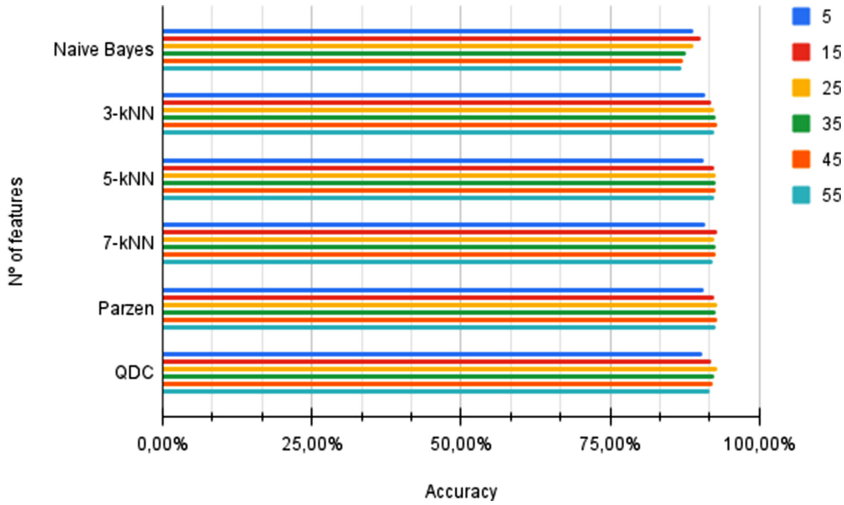

Figure 1.11. Analysis of different classifiers using larger progressive feature sets.

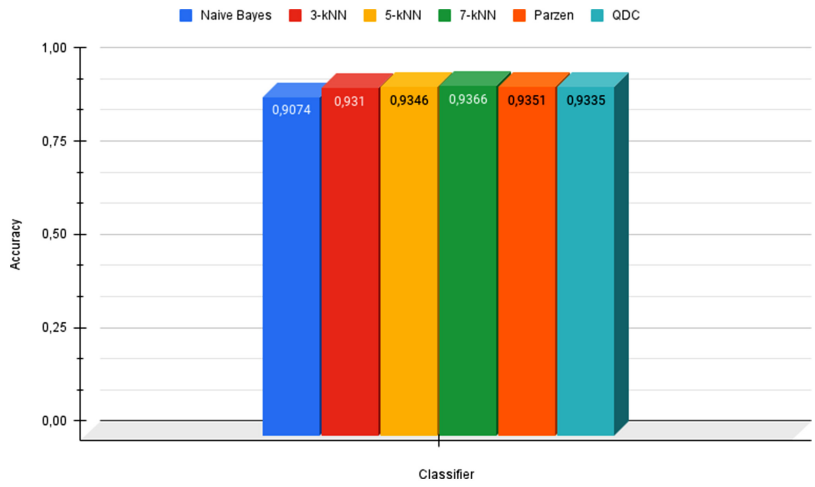

Figure 1.12. Summary of the accuracy results obtained from each classifier using the most relevant subset of features.

were obtained with the kNN algorithm with $k = 7$, reaching an accuracy value of 93.66% with only 21 features.

Using the best classifier configuration as a reference, we analyze different window sizes to determine the best way to distinguish the texture patterns that are present in the DRT edema regions of the surrounding healthy tissues. Each window has a variable height value (h) centered on the analyzed column. These h values are calculated by the distance between the ISOS and the OPL retinal layers. Figure 1.13 presents the performance of the 7-kNN learning strategy for different window sizes. Once again, satisfactory results were obtained, reaching accuracy values over 88.66%. In particular, the best values were achieved with a window size of ($h \times 23$) pixels, which resulted in an accuracy of 93.66%.

To evaluate the segmentation process, DRT identifications (SFS feature selector + 7-kNN algorithm) and their respective height values of the outer retina (distance between the ISOS and the OPL retinal layers) were used. The presented method obtained satisfactory results, achieving a 0.8381, 0.6106 and 0.7480 in Accuracy, Jaccard and Dice coefficients, respectively, without any post-processing step.

Using the segmentation of DRT regions as a reference, we tested the capabilities of both designed post-processing approaches. To do so, firstly, we analysed the first post-processing step for the reduction of the FP rates, eliminating the isolated DRT regions. As mentioned above, these false detections are generally produced by the existence of other pathological structures that may be found within the analyzed region of the retina. In particular, we analyzed the best combination between the width of the DRT regions ($w_{\min}$) and the distance to the closest DRT columns ($d_{\min}$). The results obtained provided a reasonable balance between Jaccard and Dice (0.6162 and 0.7516, respectively) using values of $w_{\min}$ and $d_{\min}$ (16 and 10, respectively).

The second post-processing step aims at the analysis of DRT columns and subsequent reduction of the FN rates, connecting nearby pathological regions using

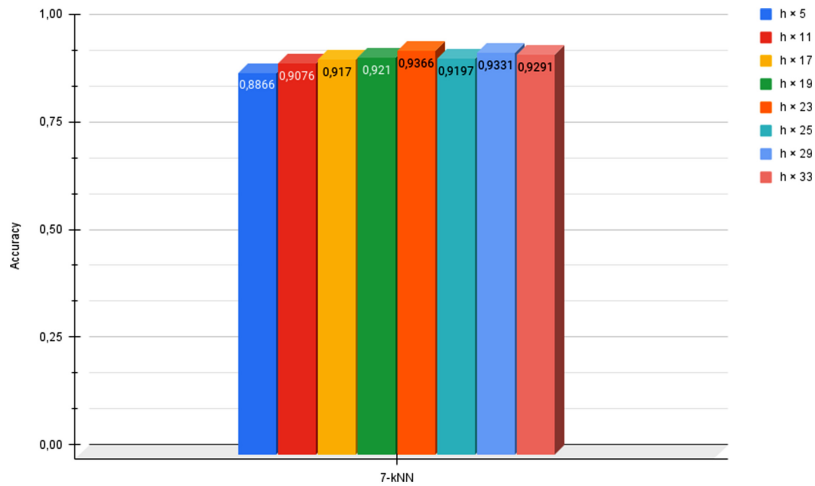

Figure 1.13. Accuracy results obtained from the 7-kNN algorithm for different window sizes.

the aggregation factor (d). As indicated, these misclassified DRT regions are mainly derived from the presence of speckle noise and/or vessel shadows. Consequently, the presented method obtained satisfactory results using an aggregation factor of 34, reaching values of 0.6625 and 0.7899 for the Jaccard and Dice coefficients, respectively.

1.4 Conclusions

This chapter presents a fully automatic system for segmentation of DRT edema in OCT images, following the reference clinical classification in ophthalmology. For this purpose, two retinal regions were defined and extracted for subsequent analysis: the ILM/OPL region (inner retina) and the OPL/RPE region (outer retina). A learning process was then applied using different classifiers to validate the appropriateness of the selected features in the segmentation of these ocular lesions. In addition, two complementary post-processing stages were designed to improve the results obtained by the presented system. This system was validated using 70 OCT scans, being 560 samples labeled to represent the presence of DRT edemas, including 280 samples for each category, DRT and non-DTR. The best result was obtained by the 7-kNN, using 21 features and a window size of ($h \times 23$) pixels, according to Jaccard and Dice (0.6625 and 0.7899, respectively) and with a combination of post-processing stages. Therefore, the presented system has demonstrated its suitability in the automatic segmentation of DRT regions in OCT scans.

Acknowledgments

This research was funded by Instituto de Salud Carlos III, Government of Spain, DTS18/00136 research project; Ministerio de Ciencia e Innovación y Universidades, Government of Spain, RTI2018–095894-B-I00 research project, Ayudas para la formación de profesorado universitario (FPU), grant reference FPU18/02271; Ministerio de Ciencia e Innovación, Government of Spain through the research project with reference PID2019-108435RB-I00; Consellería de Cultura, Educación e Universidade, Xunta de Galicia, Grupos de Referencia Competitiva, grant reference ED431C 2020/24 and through the postdoctoral grant contract reference ED481B 2021/059; Axencia Galega de Innovación (GAIN), Xunta de Galicia, grant reference IN845D 2020/38; CITIC, Centro de Investigación de Galicia reference ED431G 2019/01, receives financial support from Consellería de Educación, Universidade e Formación Profesional, Xunta de Galicia, through the ERDF (80%) and Secretaría Xeral de Universidades (20%).

References

[1] Sonka M, Hlavac V and Boyle R 2007 *Image Processing, Analysis and Computer Vision* (Berlin: Springer) 3rd edn

[2] Umbaugh S E 2010 *Digital Image Processing and Analysis: Human and Computer Vision Applications with CVIPtools* (Boca Raton, FL: CRC Press)

[3] Gunasekaran S 1996 Computer vision technology for food quality assurance *Trends Food Sci. Technol.* **7** 245–56

[4] de Moura J, Novo J, Charlón P, Barreira N and Ortega M 2017 Enhanced visualization of the retinal vasculature using depth information in OCT *Med. Biol. Eng. Comput.* **55** 2209–25
[5] Hassanein K S, Wesolkowski S, Higgins R, Crabtree R and Peng A 1997 Integrated system for automated financial document processing *25th AIPR Workshop: Emerging Applications of Computer Vision* vol 2962 (Bellingham, WA: International Society for Optics and Photonics) 202–12
[6] Salgado L, Menendez J M, Rendon E and Garcia N 1999 Automatic car plate detection and recognition through intelligent vision engineering *Proceedings IEEE 33rd Annual 1999 Int. Carnahan Conf. on Security Technology (Cat. No. 99CH36303)* (Piscataway, NJ: IEEE) 71–6
[7] Brosnan T and Sun D W 2002 Inspection and grading of agricultural and food products by computer vision systems—a review *Comput. Electron. Agric.* **36** 193–213
[8] Bebis G, Egbert D and Shah M 2003 Review of computer vision education *IEEE Trans. Educ.* **46** 2–21
[9] Schadt E E, Linderman M D, Sorenson J, Lee L and Nolan G P 2010 Computational solutions to large-scale data management and analysis *Nat. Rev. Genet.* **11** 647–57
[10] Fernández A, Ortega M, de Moura J, Novo J and Penedo M G 2019 Automatic evaluation of eye gestural reactions to sound in video sequences *Eng. Appl. Artif. Intell.* **85** 164–74
[11] Novo J, Barreira N, Penedo M G and Santos J 2012 Topological active volume 3D segmentation model optimized with genetic approaches *Nat. Comput.* **11** 161–74
[12] Novo J, Penedo M G and Santos J 2010 Evolutionary multiobjective optimization of topological active nets *Pattern Recognit. Lett.* **31** 1781–94
[13] de Moura J, Ramos L, Vidal P L, Cruz M, Abelairas L, Castro E, Novo J and Ortega M 2020 Deep convolutional approaches for the analysis of Covid-19 using chest x-ray images from portable devices *IEEE Access* **8** 195594–607
[14] de Moura J, Novo J and Ortega M 2020 Fully automatic deep convolutional approaches for the analysis of Covid-19 using chest x-ray images *Appl. Soft Comput.* **115** 108190
[15] El-Dahshan E S A, Mohsen H M, Revett K and Salem A B M 2014 Computer-aided diagnosis of human brain tumor through MRI: a survey and a new algorithm *Expert Syst. Appl.* **41** 5526–45
[16] Javaid M, Javid M, Rehman M Z U and Shah S I A 2016 A novel approach to CAD system for the detection of lung nodules in CT images *Comput. Methods Programs Biomed.* **135** 125–39
[17] Thomaes T, Thomis M, Onkelinx S, Coudyzer W, Cornelissen V and Vanhees L 2012 Reliability and validity of the ultrasound technique to measure the rectus femoris muscle diameter in older CAD-patients *BMC Med. Imaging* **12** 7
[18] Ortega M, Barreira N, Novo J, Penedo M G, Pose-Reino A and Gómez-Ulla F 2010 Sirius: a web-based system for retinal image analysis *Int. J. Med. Inform.* **79** 722–32
[19] Tavakoli M, Toosi M B, Pourreza R, Banaee T and Pourreza H R 2011 Automated optic nerve head detection in fluorescein angiography fundus images *2011 IEEE Nuclear Science Symp. Conf. Record* (Piscataway, NJ: IEEE) 3057–60
[20] de Moura J, Novo J, Rouco J, Charlón P and Ortega M 2019 Artery/vein vessel tree identification in near-infrared reflectance retinographies *J. Digit. Imaging* **32** 947–62
[21] Cabaleiro P, de Moura J, Novo J, Charlón P and Ortega M 2019 Automatic identification and representation of the cornea–contact lens relationship using AS-OCT Images *Sensors* **19** 5087
[22] de Moura J, Novo J, Ortega M and Charlón P 2016 3D retinal vessel tree segmentation and reconstruction with OCT images *Int. Conf. on Image Analysis and Recognition* (Cham: Springer) 716–26

[23] Baamonde S, de Moura J, Novo J, Charlón P and Ortega M 2019 Automatic identification and characterization of the epiretinal membrane in OCT images *Biomed. Opt. Express* **10** 4018–33
[24] Baamonde S, de Moura J, Novo J, Charlón P and Ortega M 2019 Automatic identification and intuitive map representation of the epiretinal membrane presence in 3D OCT volumes *Sensors* **19** 5269
[25] Díaz M, de Moura J, Novo J and Ortega M 2019 Automatic wide field registration and mosaicking of OCTA images using vascularity information *Procedia Comput. Sci.* **159** 505–13
[26] Huang D, Swanson E A, Lin C P, Schuman J S, Stinson W G, Chang W and Puliafito C A 1991 Optical coherence tomography *Science* **254** 1178–81
[27] Puliafito C A, Hee M R, Lin C P, Reichel E, Schuman J S, Duker J S and Fujimoto J G 1995 Imaging of macular diseases with optical coherence tomography *Ophthalmology* **102** 217–29
[28] Romero-Aroca P 2011 Managing diabetic macular edema: the leading cause of diabetes blindness *World J. Diabetes* **2** 98
[29] Otani T, Kishi S and Maruyama Y 1999 Patterns of diabetic macular edema with optical coherence tomography *Am. J. Ophthalmol.* **127** 688–93
[30] Panozzo G, Parolini B, Gusson E, Mercanti A, Pinackatt S, Bertoldo G and Pignatto S 2004 Diabetic macular edema: an OCT-based classification *Seminars in Ophthalmology* vol 19 (Milton Park: Taylor and Francis) pp 13–20
[31] de Moura J, Samagaio G, Novo J, Charlón P, Fernández M I, Gómez-Ulla F and Ortega M 2019 Automatic identification of diabetic macular edema biomarkers using optical coherence tomography scans *Int. Conf. on Computer Aided Systems Theory* (Cham: Springer) pp 247–55
[32] Gopinath K and Sivaswamy J 2018 Segmentation of retinal cysts from optical coherence tomography volumes via selective enhancement *IEEE J. Biomed. Health Inform.* **23** 273–82
[33] Schlegl T, Waldstein S M, Bogunovic H, Endstraßer F, Sadeghipour A, Philip A M and Schmidt-Erfurth U 2018 Fully automated detection and quantification of macular fluid in OCT using deep learning *Ophthalmology* **125** 549–58
[34] de Moura J, Vidal L, Novo P, Rouco J, Penedo J, Ortega M G and M 2020 Intraretinal fluid pattern characterization in optical coherence tomography images *Sensors* **20** 2004
[35] Vidal P L, De Moura J, Novo J, Penedo M G and Ortega M 2018 Intraretinal fluid identification via enhanced maps using optical coherence tomography images *Biomed. Opt. Express* **9** 4730–54
[36] Roy A G, Conjeti S, Karri S P K, Sheet D, Katouzian A, Wachinger C and Navab N 2017 ReLayNet: retinal layer and fluid segmentation of macular optical coherence tomography using fully convolutional networks *Biomed. Opt. Express* **8** 3627–42
[37] Samagaio G, Estévez A, de Moura J, Novo J, Fernández M I and Ortega M 2018 Automatic macular edema identification and characterization using OCT images *Comput. Methods Programs Biomed.* **163** 47–63
[38] de Moura J, Samagaio G, Novo J, Almuina P, Fernández M I and Ortega M 2020 Joint diabetic macular edema segmentation and characterization in OCT images *J. Digit. Imag.* **33** 1–17
[39] de Moura J, Novo J and Ortega M 2019 Deep feature analysis in a transfer learning-based approach for the automatic identification of diabetic macular edema *2019 Int. Joint Conf. on Neural Networks (IJCNN)* (Piscataway, NJ: IEEE) 1–8
[40] Chan G C, Muhammad A, Shah S A, Tang T B, Lu C K and Meriaudeau F 2017 Transfer learning for diabetic macular edema (DME) detection on optical coherence tomography

(OCT) images *2017 IEEE Int. Conf. on Signal and Image Processing Applications (ICSIPA)* (Piscataway, NJ: IEEE) 493–6

[41] de Moura J, Novo J, Charlón P, Fernández M I and Ortega M 2019 Retinal vascular analysis in a fully automated method for the segmentation of DRT edemas using OCT images *Procedia Comput. Sci.* **159** 600–9

[42] Samagaio G, de Moura J, Novo J and Ortega M 2018 Automatic segmentation of diffuse retinal thickening edemas using optical coherence tomography images *Procedia Comput. Sci.* **126** 472–81

[43] González-López A, de Moura J, Novo J, Ortega M and Penedo M G 2019 Robust segmentation of retinal layers in optical coherence tomography images based on a multistage active contour model *Heliyon* **5** e01271

[44] Samagaio G, de Moura J, Novo J and Ortega M 2017 Optical coherence tomography denoising by means of a fourier butterworth filter-based approach *Int. Conf. on Image Analysis and Processing* (Cham: Springer) 422–32

[45] Berk K N 1980 Forward and backward stepping in variable selection *J. Stat. Comput. Simul.* **10** 177–85